



Cite this: *Phys. Chem. Chem. Phys.*,  
2024, 26, 8334

# Silica nanoparticles and kaolin clay decorated with VO<sup>2+</sup> in aerobic oxidative destruction of BTEX contaminants†

Pegah Mohammadpour,<sup>a</sup> Elham Safaei<sup>\*a</sup> and  
Constantinos D. Zeinalipour-Yazdi<sup>b</sup>

The importance of controlled hydrocarbon oxidation has sparked interest in methods that catalyze this process. In this vein, controlled oxidative degradation of BTEX compounds (benzene, toluene, ethylbenzene and xylenes) which are hazardous air and industrial waste water contaminants is very considerable. Accordingly, the reactive VO<sup>2+</sup> species was anchored onto silica nanoparticles (VO–SNP) to catalyze the conversion of BTEX into useful compounds. The synthesized heterogeneous VO–SNP catalyst was characterized using different techniques such as FTIR, FETEM, FESEM, XRD, EDX, ICP and XPS. Interestingly, the catalyst performed the activation of the relatively inert C–H bonds of BTEX to produce oxygenated compounds under quite mild and eco-friendly conditions at room temperature with no extra additives. Furthermore, we introduced VO<sup>2+</sup> species onto mineral kaolin sheets (VO–kaolin) as a vanadyl decorated natural solid support and the results showed less efficiency compared to VO–SNP.

Received 31st August 2023,  
Accepted 27th November 2023

DOI: 10.1039/d3cp04218a

rsc.li/pccp

## 1. Introduction

The petroleum industry is using millions of barrels of oil daily, releasing huge amounts of contaminants and toxic chemicals into the environment.<sup>1</sup> Volatile organic compounds (VOC), such as benzene, toluene, ethylbenzene and xylene (BTEX), are the most common group of chemical pollutants released from oil industry.<sup>2</sup> Different methods have been reported for the elimination of BTEX, *e.g.*, chemical adsorption, biological treatment and oxidation processes.<sup>3</sup> The last solution is reasonably more economic due to the conversion of toxic waste materials to essential oxygenated compounds.<sup>4,5</sup> Although C–H bond oxidation reaction in these compounds is a complex process because of the inert nature of C–H bonds, the oxidative removal of BTEX is generally performed under harsh conditions such as high temperatures, with a strong oxidant or reductant, in acidic or basic media and using catalysts based on noble metals or transition metal oxides.<sup>6,7</sup> Recently, heterogeneous catalysts have been developed to direct these types of organic transformations in accordance with green chemistry through maintaining the catalyst after several catalytic

cycles.<sup>8–10</sup> On the other hand, the catalytic conversion of inactive C–H bonds should be affordable on an industrial scale with minimum material and energy consumption. Therefore, designing an efficient catalytic system that facilitates C–H bond activation under mild conditions is always required.<sup>11,12</sup>

Catalysts containing noble metals, *e.g.*, highly efficient platinum and palladium, are usually supported by earth abundant low-cost materials such as silica and aluminum oxide (γ-Al<sub>2</sub>O<sub>3</sub>).<sup>13–16</sup> For more dispersion and increasing the reactant adsorption surface, other supports have been used including MCM-41, TiO<sub>2</sub>, SBA-15, Co<sub>3</sub>O<sub>4</sub>, *etc.* While there has been research on non-noble metal based catalysts, their practical use remains constrained by various challenges, including challenging disposal methods, elevated toxicity, and reduced activity levels.<sup>14–19</sup> On the other hand, choosing an appropriate catalyst for green oxidative removal of BTEX pollutants has remained a considerable challenge. Owing to the abundance of released petroleum scraps in the environment, the oxidative transformation reactions have to be aerobic or oxygen-induced with minimum energy and chemical consumption, but there are only a few reports that introduce the ideal protocol.<sup>20–22</sup> Table 1 presents recently reported catalysts for the oxidative destruction of toluene, one of the most important BTEX pollutants.

Herein, we demonstrate a clean and cost-effective way to eliminate BTEX contaminants using a simple and efficient vanadyl-based catalyst immobilized on silica nanoparticles (VO–SNP) (Scheme 1). The remarkable results of VO–SNP

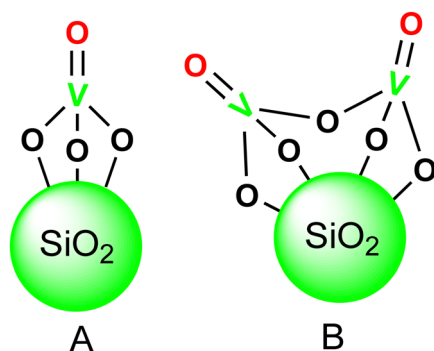
<sup>a</sup> Department of Chemistry, College of Sciences, Shiraz University, Shiraz, 7194684795, Iran. E-mail: e.safaei@shirazu.ac.ir

<sup>b</sup> Department of Natural Sciences, Middlesex University, Hendon Campus, the Burroughs, London NW4 4BT, UK

† Electronic supplementary information (ESI) available. See DOI: <https://doi.org/10.1039/d3cp04218a>

Table 1 Recent reports on oxidative degradation of toluene

Entry	Catalyst	Reaction conditions	Con. (%)	Major product
1 <sup>23</sup>	CuBr <sub>2</sub> @g-C <sub>3</sub> N <sub>4</sub> (20 mg)	Toluene (1 mmol), TBHP (3 mmol), <i>T</i> = 120 °C, time = 6 h	79	Benzaldehyde
2 <sup>24</sup>	VO(acac) <sub>2</sub> (0.0032 mmol), Co(acac) <sub>2</sub> (0.012 mmol)	Toluene (40 mmol), H <sub>2</sub> O <sub>2</sub> (40 mmol), MeCN (15 mL), <i>N</i> -hydroxyphthalimide (6 mM), <i>T</i> = 40 °C, time = 5 h	10	Benzyl alcohol
3 <sup>25</sup>	CoO <sub>x</sub> /SiO <sub>2</sub> (0.005 g)	Toluene (0.5 mmol), <i>N</i> -hydroxyphthalimide (0.05 mmol), hexafluoropropan-2-ol (1 mL), O <sub>2</sub> (0.1 MPa), <i>T</i> = RT, time = 4 h	91	Benzaldehyde
4 <sup>26</sup>	Pt <sub>28</sub> subnanocatalyst (10 mg)	Toluene (2 mL), O <sub>2</sub> (1 MPa), <i>T</i> = 160 °C, time = 15 h in an autoclave reactor	1000 μmol product	Benzoic acid
5 <sup>27</sup>	Ce <sub>0.9</sub> Bi <sub>0.1</sub> O <sub>1.8</sub> (0.1 g)	Toluene (8.3 M, 2.7 mL), TBHP (70%, 167 mM), <i>T</i> = 60 °C, time = 24 h	42	Benzaldehyde
6 <sup>28</sup>	Nano-NiFe <sub>2</sub> O <sub>4</sub> @CAGC (100 mg)	Toluene (5 mL), TBHP (3 equivalents), <i>T</i> = 120 °C, time = 12 h, two 10 W LED bulbs	1000 μmol product	Benzyl benzoate
7 <sup>29</sup>	Polystyrene grafted vanadium Schiff base complex (30 mg)	Toluene (5 mmol), CH <sub>3</sub> CN (10 mL), H <sub>2</sub> O <sub>2</sub> (15 mmol), <i>T</i> = 65 °C, time = 6 h	79	Benzaldehyde
8 <sup>30</sup>	Fe <sub>3</sub> O <sub>4</sub> @SiO <sub>2</sub> -APTES-MnL <sup>GDC</sup> (40 mg)	Toluene (1 mmol), solvent free, TBHP (4 eq., 70%), <i>T</i> = 60 °C, time = 20 h	71	Benzoic acid
9 <sup>31</sup>	VO <sup>2+</sup> @SiO <sub>2</sub> @Fe <sub>3</sub> O <sub>4</sub> (40 mg)	Toluene (1 mmol), TBHP (2 mmol), H <sub>2</sub> O (0.5 mL), Ar atmosphere, <i>T</i> = RT, time = 8 h	99	Benzoic acid
10 <sup>32</sup>	fcc Ni catalyst (6 mg)	Toluene (5 mL), 0.5 mL water (additive), phenyliodine(III) diacetate (50 mg), reflux temperature, time = 60 minutes	80	Benzyl alcohol
11 <sup>33</sup>	(Fe,Co,Ni,Cu) <sub>3</sub> O <sub>4</sub> @rGO (0.016 g)	Toluene (3 mL), air (10 atm), <i>T</i> = 125 °C, time = 4 h	18.2	Benzaldehyde
12 <sup>34</sup>	BiOCl/TiO <sub>2</sub> (25 mg)	Toluene (1 mmol), MeCN (3 mL), O <sub>2</sub> (1 atm), λ > 320 nm, time = 2 h	10	Benzaldehyde
This work	VO <sup>2+</sup> @SNP (50 mg)	Toluene (1 mmol), H <sub>2</sub> O (0.5 mL), oxygen balloon, <i>T</i> = RT, time = 8 h	100	Benzyl alcohol

Scheme 1 Molecular structure of VO-SNP. (A) The monomer form and (B) the dimer form. Green particles of SiO<sub>2</sub> are 200 nm in diameter.

strongly motivated us to modify the catalyst and suggest it to modify the catalyst and bring it closer to the industrial use. Unlike most of the prior reports, VO-SNP is impressive and sustainable enough to perform oxidative activation of the C-H bonds of aromatic hydrocarbons in the presence of an oxygen atmosphere, in water medium and under room temperature conditions. After performing experimental research on different natural mineral clays, we used the natural kaolin clay powder to stabilize VO<sup>2+</sup> in order to support the V=O species and prepare a more cost-effective and green catalyst named VO-kaolin. In fact, V=O terminal bonds in supported vanadia catalysts are anticipated as effective sites in many oxidation reactions to involve active oxygen atoms. In addition, V=O is a good alternative for noble metal containing catalysts as a potential oxygen source to facilitate oxidation transformation. The observed high conversion and excellent selectivity motivated us to use kaolin as a natural and completely clean support

without any synthetic waste production. This survey focused on reducing BTEX through oxidative degradation in a completely environmentally-friendly scaffold using a simple synthetic heterogeneous catalyst with the slightest chemical ingestion. Moreover, the results are notable because of high selectivity owing to the controllable oxidation process that does not generate over-oxidation products.

## 2. Results and discussion

### 2.1. Catalyst characterization

It has been demonstrated that the VO<sup>2+</sup> ion can attach to a SiO<sub>2</sub> surface in a tetrahedral configuration in monomer [VO<sub>4</sub>] or dimer [V<sub>2</sub>O<sub>7</sub>] forms (Scheme 1).<sup>35–37</sup> This is achieved through the reaction of the highly reactive VOCl<sub>3</sub> with the Si-OH groups on the silica surface. Subsequently, HCl is released in an inert atmosphere, allowing VO<sup>2+</sup> to become immobilized on the silica surface by forming three V-O bonds. The successful stabilization of VO<sup>2+</sup> species on silica and kaolin is investigated through different analytical and spectroscopic methods. In the FT-IR spectra of VO-SNP, the bands at 471 cm<sup>-1</sup> and 802 cm<sup>-1</sup> are respectively assigned to Si-O-Si bending and Si-O-Si stretching vibrations, while the sharp peak at 1104 cm<sup>-1</sup> refers to the siloxane vibration of (SiO)<sub>n</sub> groups. The absorption bands at 1637 cm<sup>-1</sup> and 3406 cm<sup>-1</sup> are attributed to the adsorbed water molecules and O-H stretching bands of the silica surface, respectively. The noticeable peak at 944 cm<sup>-1</sup> confirms the V=O stretching bands of VO-SNP.<sup>38</sup> On the other hand, the peaks at 3600 cm<sup>-1</sup> and 1600 cm<sup>-1</sup> in the FT-IR spectra of VO-kaolin are correlated to the O-H stretching and H-O-H bending, respectively (Fig. S1b, ESI<sup>†</sup>). The strong bands at

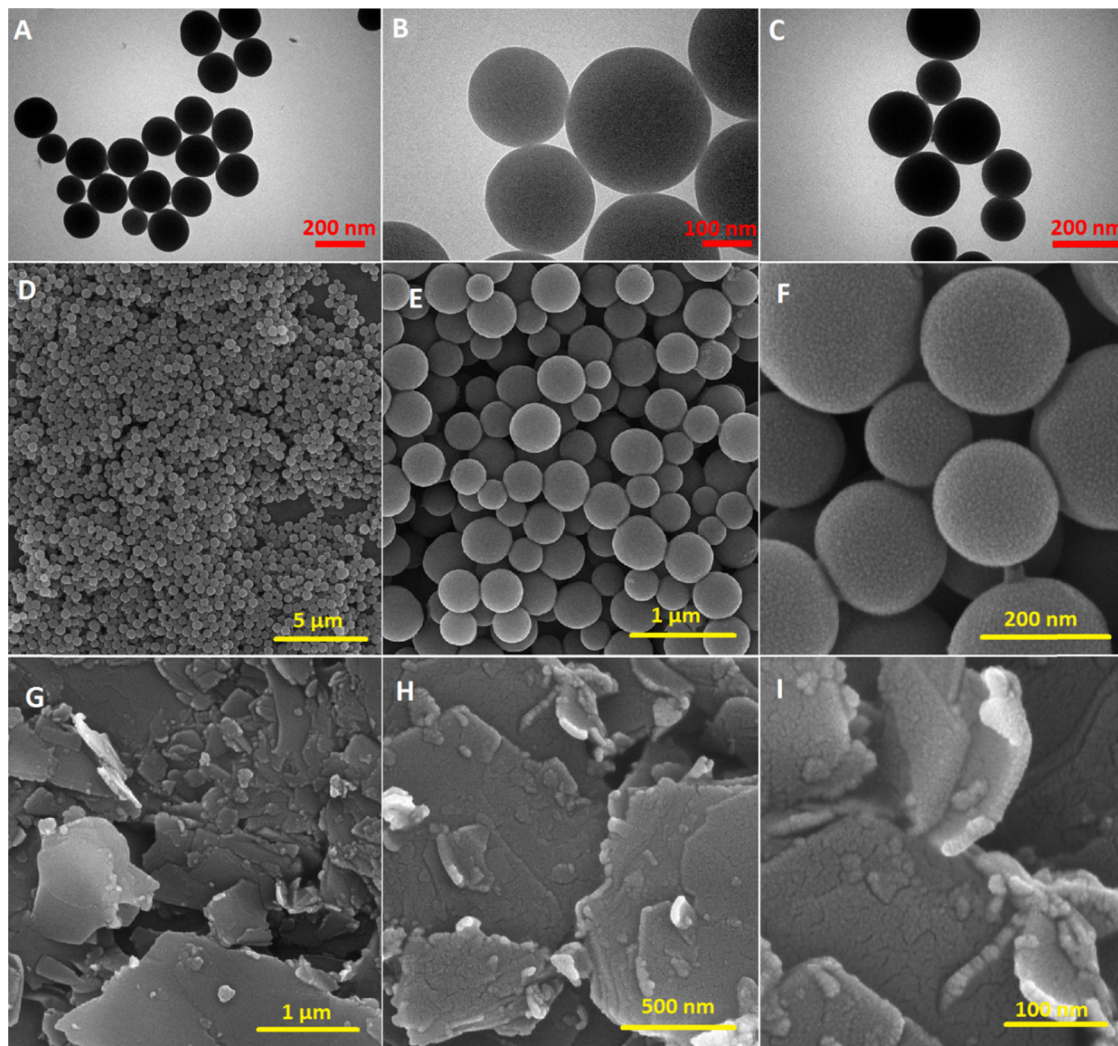


Fig. 1 FETEM images of VO-SNP: (A) 200 nm, (B) 100 nm, and (C) after recycling; FESEM images of VO-SNP: (D) 5  $\mu\text{m}$ , (E) 1  $\mu\text{m}$ , and (F) 200 nm; FESEM images of VO-kaolin: (G) 1  $\mu\text{m}$ , (H) 500 nm, and (I) 200 nm.


1070  $\text{cm}^{-1}$  and 480  $\text{cm}^{-1}$  are attributed to the Si–O–Si groups of tetrahedral sheets. The peak at 540  $\text{cm}^{-1}$  reflects Al–O bending and the spectral signal at 810  $\text{cm}^{-1}$  is attributed to the stretching vibration of Si–O. The successful stabilization of  $\text{VO}^{2+}$  on mineral kaolin is confirmed through the appearance of a  $\text{V}=\text{O}$  stretching bond at 950  $\text{cm}^{-1}$  in the FTIR spectrum.

The dispersion and morphology of the catalysts are investigated using field-emission transmission electron microscopy (FE-TEM) and field-emission scanning electron microscopy (FE-SEM) techniques. The totally uniform distribution of spherical silica nanoparticles is the first thing that is noticed (Fig. 1A and B). According to the FE-TEM results, the average size of silica nanoparticles is estimated as  $\sim 200$  nm, which indicates the orderly dispersion of VO-SNP. On the other hand, the good stability of shape and configuration of recovered VO-SNP represent the sustainable function during the catalytic process (Fig. 1C). The FE-SEM images of VO-SNP demonstrate the spherical structures of nanoparticles at all three different resolutions (Fig. 1D–F).

Additionally, the hexagonal crystallized morphology and thickness of VO-kaolin particles are revealed in Fig. 1G–I.

The elemental composition of VO-SNP and VO-kaolin was determined using energy-dispersive X-ray spectroscopy (EDX) (Fig. S2, ESI<sup>†</sup>) and the counts of elements could apparently determine the catalyst formation. Furthermore, the quantity of incorporated vanadium was measured by inductively coupled plasma optical emission spectroscopy (ICP-OES); the results were in good agreement with the EDX graphs (1.6  $\text{mmol g}^{-1}$  for VO-SNP and 1.1  $\text{mmol g}^{-1}$  for VO-kaolin). The X-ray powder diffraction patterns of the catalysts were recorded to define the crystalline structures. The presence of a broad peak in the XRD spectrum of VO-SNP at  $2\theta = 22^\circ$  was the evidence of the amorphous nature of the nano-silica lattice (Fig. S3, ESI<sup>†</sup>).<sup>39</sup> From the X-ray photoelectron spectroscopy (XPS) results, the spin-orbit coupling phenomena caused the  $\text{V}2\text{p}$  splitting in the vanadium dioxide. The binding energies at 518 eV and 521 eV were ascribed to  $\text{V}2\text{p}_{3/2}$  and  $\text{V}2\text{p}_{1/2}$ , respectively, which

Table 2 Optimization of catalytic activity in toluene oxidation reaction



Entry	Catalyst (mg)	Water (mL)	Time (h)	% conversion	% selectivity
1	20	0.5	8	38	>99
2	30	0.5	8	39	>99
3	40	0.5	8	52	>99
4	50	0.5	8	92	>99
5	50	0.3	8	91	>99
6	50	1	8	89	>99
7	50	0.5	7	93	>99
8	50	0.5	6	92	>99
9	50	0.5	10	94	>99

endorsed the oxidation state of +5 with vanadium (Fig. S4, ESI<sup>†</sup>).<sup>40</sup>

## 2.2. Catalytic evaluation of BTEX removal using VO-SNP


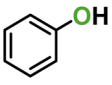
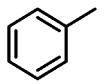
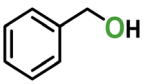
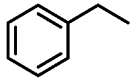
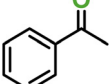
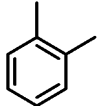
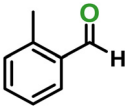
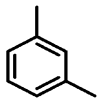
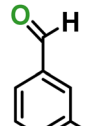
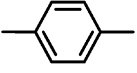
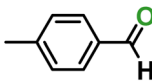
According to the emphasis on green transformation of BTEX pollutants and the importance of clean production of oxygenated compounds and also due to the high potential of oxygen atom activity in V=O, we have carried out the catalytic reactions under economical and eco-friendly conditions. Different reaction parameters were applied for the toluene oxidation reaction (Table 2) and the reactions were carried out under an oxygen atmosphere using water solvent at room temperature. According to the gas chromatography (GC) and thin layer

chromatography (TLC) investigations, the reaction was completed in six hours under optimized conditions and the reaction process did not proceed remarkably in 7, 8 or 10 hours (Table 2, entries 7–9). For the best toluene conversion, a minimum of 50 mg of catalyst was essential and applying less mol% of catalyst reduced the catalyst efficiency remarkably (Table 2, entries 1–4). The conversions were not affected significantly by the volume of water (Table 2, entries 5 and 6), while the observed conversion was only 13% in the absence of an oxygen balloon after even 18 hours. Interestingly, the selectivity in all cases was perfect and was not affected by the applied conditions. The oxidation process stopped after the first step of oxidation progression and led to a pure product (benzyl alcohol) which was considered a great improvement in oxidation reactions. In general, benzyl alcohol is a known solvent in many industries and an essential precursor, especially for the synthesis of a wide range of ethers and esters.

We applied the obtained optimized conditions to green transformation of benzene, ethylbenzene and xylenes (Table 3). Benzene oxidation reaction using the mild standard conditions was not performed and only at high temperatures (120 °C) a 13% conversion was achieved due to the strength of arene sp<sup>2</sup> C–H bonds in comparison to benzylic sp<sup>3</sup> C–H bonds (20–30 kcal.mol<sup>-1</sup>).

However, ethylbenzene oxidation reaction was entirely accomplished with excellent conversion and selectivity and a smaller reaction time. Apparently, this improvement in the ethylbenzene reaction performance was addressed in the C–H bond strength order of aryl > 1° > 2° >> 3° and the preference

Table 3 BTEX oxidation degradation reactions

Entry	Substrate	Product	Time (h) (VO-SNP, VO-kaolin)	Conversion (%) (VO-SNP, VO-kaolin)	Selectivity (%) (VO-SNP, VO-kaolin)
B			20, 24	13, N.R.	>99, >99
T			8, 9	100, 92	>99, >99
E			7, 7	100, 100	>99, >99
X			14, 17	78, 69	>99, >99
X			16, 17	63, 60	>99, >99
X			13, 13	86, 77	>99, >99

Reaction conditions: VO-SNP (50 mg) or VO-kaolin (72 mg), H<sub>2</sub>O (0.5 mL), oxygen balloon, T = RT.

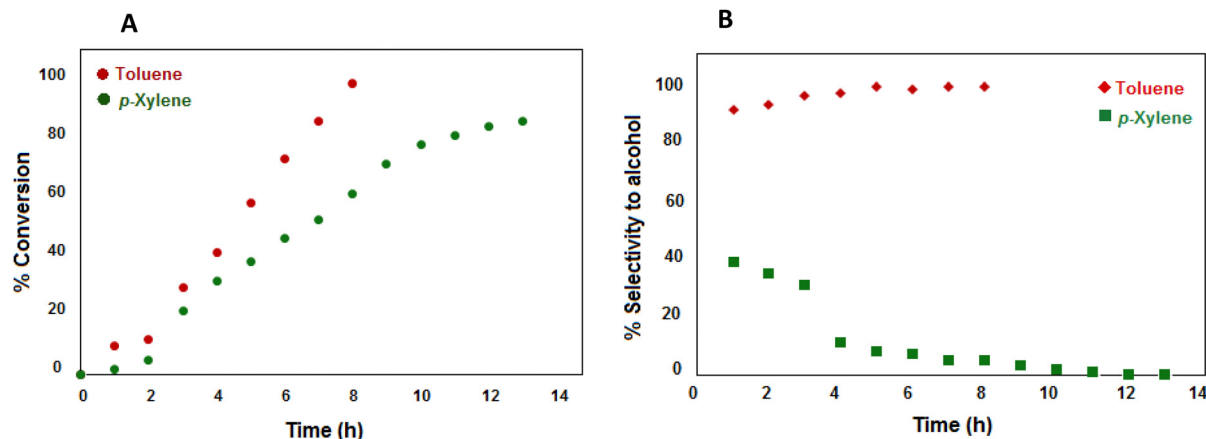


Fig. 2 Time monitoring of (A) conversion and (B) selectivity of toluene and *p*-xylene oxidation reactions.

for the secondary C–H bond *versus* primary C–H bond is observable.<sup>41</sup>

Compared to toluene, xylenes were shown to have an enhanced tendency of overoxidation on account of bearing two electron donating methyl groups, and high selectivity was obtained for oxidation of only one methyl group to aldehyde. The second methyl group remained inactive probably because of the electron withdrawing effect of the carboxyl group. Alternatively, *ortho* and *para* isomers were able to achieve a higher conversion compared to the *meta* one.

Fig. 2 compares the toluene and *p*-xylene conversion and selectivity reaction progression. According to Fig. 2A, toluene conversion increases with a sharper slope than that of *p*-xylene, but both display a sharp rise in the first 3–4 hours of reaction. In contrast, the selectivity for benzyl alcohol production remains maximum with a constant slope, while the selectivity for *p*-tolylmethanol levels off after 4 hours, confirming the satisfactory selectivity of 4-methylbenzaldehyde (Fig. 2B).

### 2.3. Catalytic activity of VO<sup>2+</sup> stabilized on natural kaolin

Kaolin is a natural mineral clay with the chemical composition Al<sub>2</sub>Si<sub>2</sub>O<sub>5</sub>(OH)<sub>4</sub> and a layered crystalline structure of a tetrahedral sheet of silicate (SiO<sub>4</sub>) connected with oxygen atoms to an octahedral sheet of alumina (AlO<sub>6</sub>) (Fig. 3).<sup>42</sup> Comparing to other clays, kaolin is a soft and fine powder which is easily dispersed in water. The abundance of OH groups on the surface of kaolin makes it suitable for stabilization of VO<sup>2+</sup> ions. Pure kaolin is composed of 46% silicate, 40% alumina and 14% water.<sup>43</sup> According to the ICP results, relatively good loading for VO<sup>2+</sup> ions (1.1 mmol g<sup>-1</sup>) was confirmed. For better evaluation, the optimized conditions for catalysis using VO-kaolin were the same as those for VO-SNP. However, the observed efficiency of VO-SNP was slightly better in conversion and similar in total selectivity (Table 3). The improved function of silica could possibly be related to nano-size spherical silica particles that cause an increase in the dispersion and collision of heterogeneous catalyst and substrate molecules in reaction media. Table 3 provides the conversion and selectivity values for the scope of BTEX oxidation reactions by means of VO-kaolin.

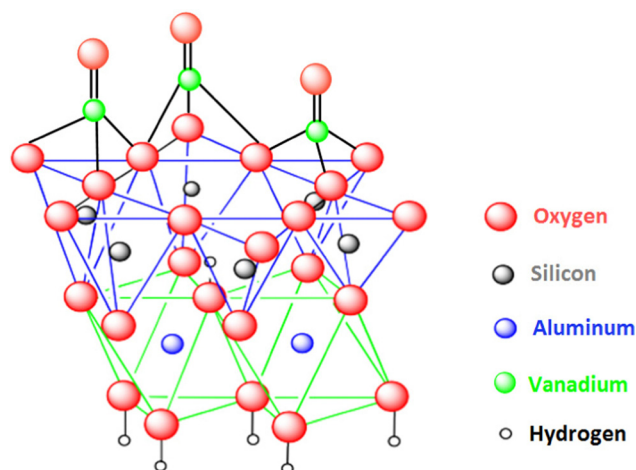
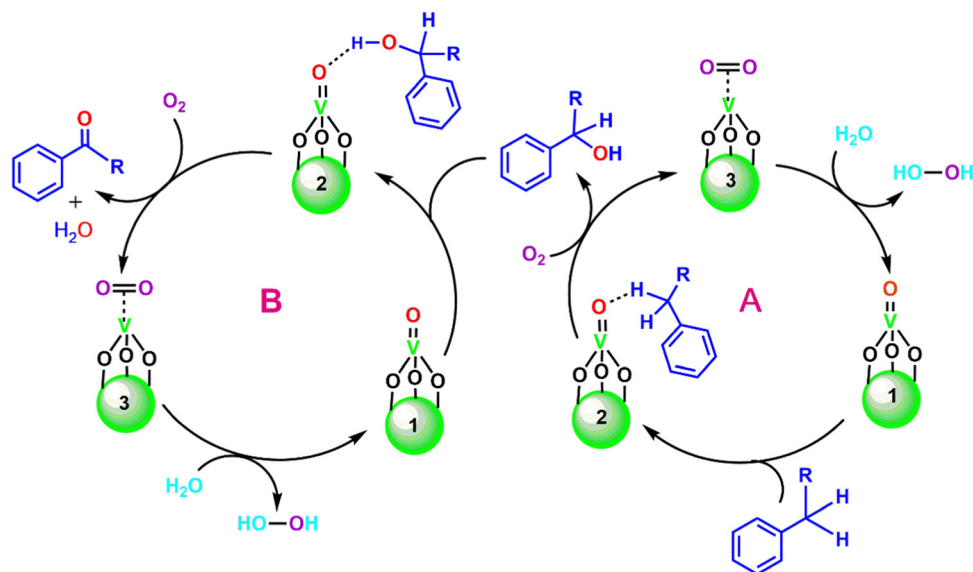


Fig. 3 Molecular structure of VO-kaolin.

### 2.4. The hypothetical mechanism of aerobic oxidation of BTEX

The totally aerobic oxidation of the most contaminated compounds (*e.g.* BTEX) is interesting mechanistically. In fact, the oxygen spin state is triplet (<sup>3</sup>O<sub>2</sub>p), while it is singlet for most of the organic compounds. Consequently, the difference in spin states creates a large activation energy barrier which makes the reaction progress very hard. Generally, these oxygen-induced reactions require high temperatures to relieve the peak of energy.<sup>44,45</sup> Nevertheless, the key role of V=O as the active site of the catalytic cycle is undeniable.

Initially, the hydrogen bonding interactions occur between the methyl hydrogen atom in toluene and the vanadyl oxygen atom (Scheme 2A). Then, the insertion of the vanadyl oxygen atom into the C–H bond was followed by the replacement of O<sub>2</sub> due to the large concentration of oxygen in reaction media. To acquire excellent selectivity, the lowest possible contact of the product with the catalyst was necessary and indeed the supported catalyst could help this. The mechanism was completed by the reaction of H<sub>2</sub>O with the weak bond of O=O (as a result



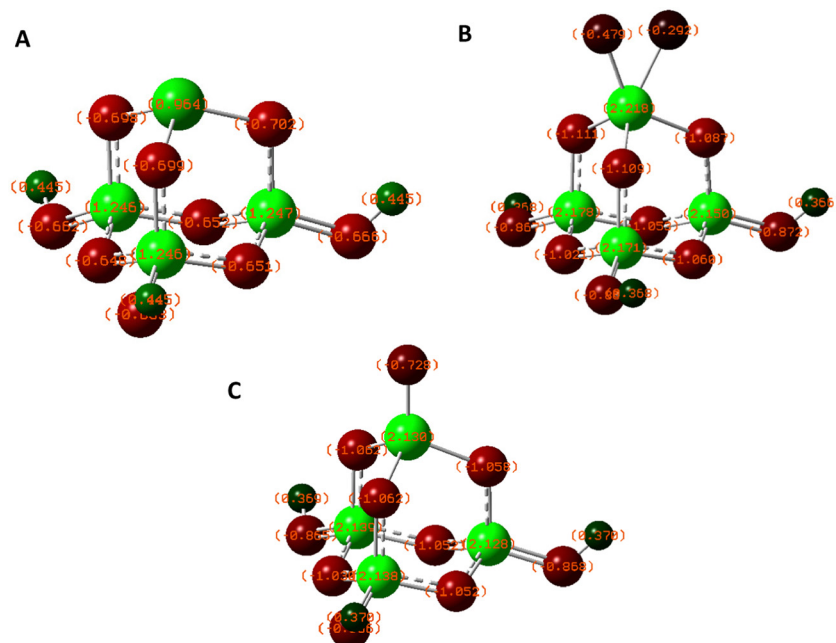
**Scheme 2** Simplified schematic of suggested mechanism of aerobic catalytic oxidation of toluene (cycle A) and ethylbenzene and xylene (cycles A and B).

of the vanadium  $\pi$ -interaction) in adduct 3 to produce H<sub>2</sub>O<sub>2</sub>, and thus the catalyst was recovered. Additionally, the presence of one methyl group and the produced hydrogen peroxide motivated the xylenes to oxidize one more time (Scheme 2B). On the other hand, using TEMPO (1 equivalent) as a common radical scavenger led to rejection of the radical chain hypothesis and the evidence was in agreement with the proposed mechanism shown in Scheme 2. However, the mechanism is only a suggestion, and there are no claims associated with it.

## 2.5. Modeling of the catalytic site *via* DFT

In order to understand the mechanism of oxidation that the catalyst undergoes, we have calculated at the B3LYP/6-31G(d) (5d, 7f) level of theory the ATP partial charges on the atoms, which are shown in Fig. 4. Our calculations indicate that the catalyst can exist in two oxidation states.

Our cluster model has the stoichiometry VO–SNP, but the dangling bonds on the oxygens have been saturated with hydrogens in order to give the stoichiometry VO<sub>3</sub>SiO<sub>3</sub>(OH)<sub>3</sub>. We find that upon adsorption O<sub>2</sub> becomes nucleophilic as it



**Fig. 4** Ball-and-stick schematic of the cluster model of the VO–SNP catalyst used in this study and its various oxidation states: (A) V, (B) VO<sub>2</sub> and (C) VO.

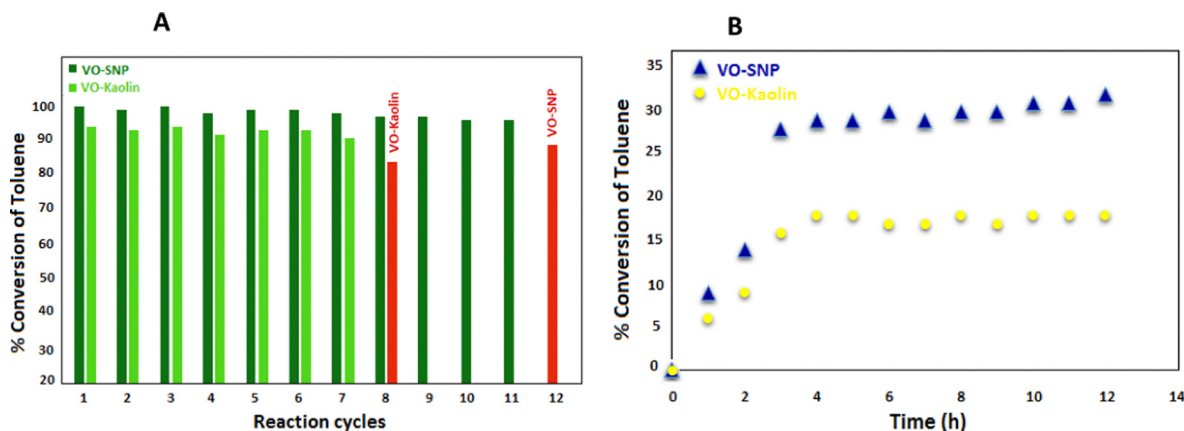


Fig. 5 (A) Reusability experiments for toluene oxidation using VO-SNP and VO-kaolin and (B) hot filtration test.

has an ATP charge of  $-0.292e$  and  $-0.479e$  on the two oxygens. Furthermore, the O=O bond weakens considerably as its length becomes  $1.438 \text{ \AA}$  when  $\text{O}_2$  is adsorbed to the catalyst compared to  $1.216 \text{ \AA}$  when it is in the gas phase. We observe that the adsorption of O to the vanadium atom has a considerable effect on the oxidation state of the catalyst, which is suggested by the change in the ATP partial charges. We find that there are two oxidation states of the catalyst: the VO cluster ( $2.130e$ ) and  $\text{VO}_2$  cluster ( $2.218e$ ) having the same oxidation state and the free catalytic site V ( $0.964e$ ) which has a different oxidation state.

### 2.6. Reusability and leaching measurements of VO-SNP and VO-kaolin catalysts

To explore the recyclability and sustainability of VO-supported catalysts, the catalyst nanoparticles were separated by centrifugation after each catalytic cycle, washed with ethanol, and dried in vacuum at  $80 \text{ }^\circ\text{C}$  overnight for the next cycle. Fig. 5A shows the recovery cycles of catalysts. VO-SNP shows 11 recovery cycles without any significant decrease in efficacy, while this number for VO-kaolin was only seven which shows the important role of support in turnover stability. The strength of  $\text{VO}^{2+}$  ion binding to the  $-\text{OH}$  groups of silica and kaolin was examined by leaching tests. The oxidation reaction of toluene was stopped after three hours, then the catalyst was isolated by centrifugation and the reaction solution was kept under stirring for eight hours. The amount of leached catalyst was measured by ICP with negligible results for both VO-SNP and VO-kaolin catalysts ( $0.0107$  and  $0.011 \text{ mmol g}^{-1}$ , respectively), which verified that  $\text{VO}^{2+}$  ions were covalently bonded to the  $\text{SiO}_2$  nanoparticles. Furthermore, the GC studies indicated that the conversion stopped after two hours and then heterogeneously continued after this period (Fig. 5B).

## 3. Conclusion

In this study, we introduced an inexpensive and eco-friendly heterogeneous catalytic system for oxidative degradation of the most common and volatile petroleum industrial pollutants. By

the suitable immobilization of  $\text{VO}^{2+}$  species on the  $-\text{OH}$  groups of the silica surface, a sustainable and active catalyst was prepared to transfer the oxygen into the strong C-H bonds under green conditions. We also applied natural and clean kaolin to support  $\text{VO}^{2+}$  ions onto alumina sheets to reduce chemical consumption and waste production. Under totally mild conditions, the excellent selectivity in obtaining one product was achieved with both supported catalysts, but lower conversion was observed for VO-kaolin owing to the plane morphology and larger size than uniform spherical silica nanoparticles. Xylenes through methyl-assisted and ethylbenzene *via* more active  $2^\circ$  C-H bonds oxidized the C-H bonds to C=O instead of C-OH. The hot filtration test indicated that the catalytic process was accomplished heterogeneously. On the other hand, the high recovery cycles of VO-SNP compared to VO-kaolin indicated synthetic silica as a robust and efficient heterogeneous base. So the oxidative removal of BTEX contaminants was achieved, which provided a guideline to prepare effective and green catalysts for catalytic BTEX degradation.

## 4. Experimental

### 4.1. Materials and characterization setup

All materials and solvents of commercial analytical grade were obtained from Sigma-Aldrich and Merck and used without further purification. Fourier transform infrared (FT-IR) spectra from KBr pellets of the compounds were recorded using a Shimadzu FT-IR-8300 spectrophotometer (Japan). Transmission electron microscopy (TEM) was carried out using field-emission transmission electron microscope (JEOL, JEM-2100F,  $200 \text{ kV}$ ) and the scanning electron microscopy (SEM) images were taken using a field-emission scanning electron microscope (Hitachi S-4800, Japan). Besides, the reactions were monitored using thin layer chromatography (TLC) and gas chromatography (GC, Agilent gas chromatograph; model: 7890A, United States) with an HP-1 methyl siloxane column ( $30 \text{ m} \times 320 \text{ } \mu\text{m} \times 0.25 \text{ } \mu\text{m}$ ) attached to a flame ionization detector (FID). The X-ray powder diffraction patterns were obtained using a PHILIPS PW1730 (step size:  $0.05$ , time per step:  $1 \text{ s}$ ). The electronic states of the powders

were evaluated by using XPS (MultiLab 2000, Thermo Scientific, Al-Ka radiation, United States).

#### 4.2. Computational methods

All calculations were performed with Gaussian using the B3LYP functional.<sup>46,47</sup> Atomic partial charges were calculated with the atomic polar tensor (APT) method<sup>48</sup> at the B3LYP/6-31G(d) (5d, 7f) level of theory.

#### 4.3. Synthesis of silica nanoparticles

SiO<sub>2</sub> nanoparticles were synthesized with a simple procedure.<sup>49,50</sup> Briefly, in a 250 mL round-bottom flask, 3.4 mL aqueous ammonia was added to a solution of 74.0 mL ethanol and 10.0 mL deionized water. After that, 6.0 mL tetraethyl orthosilicate (TEOS) was added slowly at 298 K and the reaction mixture was stirred continuously for 1 hour to form white uniform silica nanoparticles. The resulting product was washed, centrifuged three times with water and ethanol and dried at room temperature.

#### 4.4. Synthesis of VO-SNP catalyst

Immobilization of VO<sup>2+</sup> on silica nanoparticles or kaolin was performed for silica materials using a reported protocol.<sup>51</sup> The air-sensitive VOCl<sub>3</sub> (0.1 mL) was added dropwise to a suspension of 1.0 g silica nanoparticles or natural kaolin and dry dichloromethane in an argon-filled glove box. The reaction mixture was stirred under an argon atmosphere for three days at room temperature. The resultant material was centrifuged and washed several times with dichloromethane, acetone and ethanol. The obtained light green powder was dried at room temperature (1.6 mmol g<sup>-1</sup> of VO-SNP).

#### 4.5. Synthesis of VO-kaolin catalyst

Following the same procedure as that of the synthesis of VO-SNP, in an argon-filled glove box, a suspension containing 1.0 gram of natural kaolin and dry dichloromethane was prepared. 0.1 mL of air-sensitive VOCl<sub>3</sub> was added dropwise to the suspension and the reaction mixture was stirred continuously under an argon atmosphere for a period of four days at room temperature. After completion of the reaction, the resulting material was separated by centrifugation and the separated material was then subjected to multiple washes using dichloromethane, followed by acetone and ethanol. Finally, the obtained product, which had a pale green appearance, was allowed to dry at room temperature (1.1 mmol g<sup>-1</sup> of VO-kaolin).

#### 4.6. General procedure for aerobic oxidation of BTEX using VO-SNP and VO-kaolin

To a 5 mL round-bottom flask, 50 mg catalyst, 1 mmol of BTEX chemical (benzene, toluene, ethylbenzene and xylene) and oxygen-saturated water (prepared by purging of oxygen gas) were added. The reaction mixture was stirred under an oxygen atmosphere (using a balloon filled with oxygen gas) and monitored with TLC and GC. Finally, the reaction was extracted with ethyl acetate, and the solid catalyst was isolated and recovered

by centrifugation and washed with a range of solvents (hexane, dichloromethane, methanol and ethyl acetate), dried and reused in another catalytic reaction. Moreover, the organic phase in ethyl acetate was evaporated, purified by thin layer chromatography and identified by <sup>1</sup>H NMR spectroscopy.

## Conflicts of interest

There are no conflicts to declare.

## Acknowledgements

The authors are grateful to the Department of Chemistry, Shiraz University for their support. E. Safaei appreciate Dr. Abbas Amini for providing valuable comments on the manuscript.

## References

- 1 D. Atoufi and H. Lampert, DJ. Impacts of oil and gas production on contaminant levels in sediments, *Curr. Pollut. Rep.*, 2020, **6**, 43–53.
- 2 Z. Mo, S. Lu and M. Shao, Volatile organic compound (VOC) emissions and health risk assessment in paint and coatings industry in the Yangtze River Delta, China, *Environ. Pollut.*, 2021, **269**, 115740.
- 3 S. Ghafoori, M. Omar, N. Koutahzadeh, S. Zendejboudi, R. N. Malhas, M. Mohamed, S. Al-Zubaidi, K. Redha, F. Baraki and M. Mehrvar, New advancements, challenges, and future needs on treatment of oilfield produced water: A state-of-the-art review, *Sep. Purif. Technol.*, 2022, **289**, 120652.
- 4 M. Coha, G. Farinelli, A. Tiraferri, M. Minella and D. Vione, Advanced oxidation processes in the removal of organic substances from produced water: Potential, configurations, and research needs, *Chem. Eng. J.*, 2021, **414**, 128668.
- 5 S. S. Stahl and P. L. Alsters, *Liquid Phase Aerobic Oxidation Catalysis: industrial applications and academic perspectives*, 2016.
- 6 M. Moselage, J. Li and L. Ackermann, Cobalt-catalyzed C–H activation, *ACS Catal.*, 2016, **6**, 498–525.
- 7 B. Yu, Z. Yuan, Z. Yu and F. Xue-song, BTEX in the environment: An update on sources, fate, distribution, pretreatment, analysis, and removal techniques, *Chem. Eng. J.*, 2022, **435**, 134825.
- 8 B. J. Gallon, R. W. Kojima, R. B. Kaner and P. L. Diaconescu, Palladium nanoparticles supported on polyaniline nanofibers as a semi-heterogeneous catalyst in water, *Angew. Chem., Int. Ed.*, 2007, **46**(38), 7251–7254.
- 9 C. Liang, C. Li, Y. Zhu, X. Du, C. Yao, Y. Ma and J. Zhao, Recent advances of photocatalytic degradation for BTEX: Materials, operation, and mechanism, *Chem. Eng. J.*, 2023, **455**, 140461.
- 10 C. I. Olivares, S. Yi, E. K. Cook, Y. J. Choi, R. Montagnolli, A. Byrne, C. P. Higgins, D. L. Sedlak and L. Alvarez-Cohen, Aerobic BTEX biodegradation increases yield of perfluoroalkyl



- carboxylic acids from biotransformation of a polyfluoroalkyl surfactant, 6: 2 FTTaOS, *Environ. Sci.: Processes Impacts*, 2022, **24**(3), 439–446.
- 11 X. Cui, R. Huang and D. Deng, Catalytic conversion of C1 molecules under mild conditions, *EnergyChem*, 2021, **3**(1), 100050.
  - 12 S. Verma, R. B. Nasir Baig, M. N. Nadagouda, R. S. Varma and C.-H. Photocatalytic, Activation of Hydrocarbons over VO@g-C<sub>3</sub>N<sub>4</sub>, *ACS Sustainable Chem. Eng.*, 2016, **4**(4), 2333–2336.
  - 13 R. El Khawaja, S. Sonar, T. Barakat, N. Heymans, B. L. Su, A. Löfberg, J. F. Lamonier, J. M. Giraudon, G. De Weireld, C. Poupin and R. Cousin, VOCs catalytic removal over hierarchical porous zeolite NaY supporting Pt or Pd nanoparticles, *Catal. Today*, 2022, **405**, 212–220.
  - 14 J. A. Labinger, Platinum-catalyzed C–H functionalization, *Chem. Rev.*, 2017, **117**(13), 8483–8496.
  - 15 O. R. Schade, K. F. Kalz, D. Neukum, W. Kleist and J. D. Grunwaldt, Supported gold-and silver-based catalysts for the selective aerobic oxidation of 5-(hydroxymethyl) furfural to 2,5-furandicarboxylic acid and 5-hydroxymethyl-2-furancarboxylic acid, *Green Chem.*, 2018, **20**(15), 3530–3541.
  - 16 Z. Liu, Y. Zhang, S. Jiang, S. Liu, J. Cao and Y. Ai, Enhanced catalytic performance and reduced by-products emission on plasma catalytic oxidation of high-concentration toluene using Mn-Fe/rGO catalysts, *J. Environ. Chem. Eng.*, 2022, **10**(6), 108770.
  - 17 T. Tabakova, P. Petrova, Y. Karakirova, G. Avdeev, E. Kolentsova and L. Ilieva, Tuning the Cu/Ce Ratio for Improved Benzene Oxidation over Gold-Promoted Alumina-Supported CuO-CeO<sub>2</sub>, *Symmetry*, 2023, **15**(2), 263.
  - 18 M. Sutradhar, M. G. Martins, D. H. Simoes, R. M. Serôdio, H. M. Lapa, E. C. Alegria, M. F. da Silva and A. J. Pombeiro, Ultrasound and photo-assisted oxidation of toluene and benzyl alcohol with oxidovanadium(v) complexes, *Appl. Catal., A*, 2022, **638**, 118623.
  - 19 E. Janiszewska, A. Held, K. Nowińska and S. Kowalak, One-pot synthesis of vanadium-containing silica SBA-3 materials and their catalytic activity for propene oxidation, *RSC Adv.*, 2019, **9**(9), 4671–4681.
  - 20 J. Huo, J. P. Tessonnier and B. H. Shanks, Improving hydrothermal stability of supported metal catalysts for biomass conversions: a review, *ACS Catal.*, 2021, **11**(9), 5248–5270.
  - 21 M. H. El-Naas, J. A. Acio and A. E. El Telib, Aerobic biodegradation of BTEX: progresses and prospects, *J. Environ. Chem. Eng.*, 2014, **2**(2), 1104–1122.
  - 22 J. Liu, A. Guðmundsson and J. E. Bäckvall, Efficient aerobic oxidation of organic molecules by multistep electron transfer, *Angew. Chem., Int. Ed.*, 2021, **60**(29), 15686–15704.
  - 23 P. Rani Verma, S. Payra, F. Khan, S. Penta and S. Banerjee, CuBr<sub>2</sub>@g-C<sub>3</sub>N<sub>4</sub>-Catalyzed Highly Selective Aerobic Oxidation of Alcohol and Toluene Derivatives, *ChemistrySelect*, 2020, **5**(6), 1950–1955.
  - 24 M. Tan, L. Zhu, H. Liu, Y. Fu, S. F. Yin and W. Yang, Microporous cobaltporphyrin covalent polymer mediated Co<sub>3</sub>O<sub>4</sub>@ PNC nanocomposites for efficient catalytic CH bond activation, *Appl. Catal., A*, 2021, **614**, 118035.
  - 25 J. Xu, G. Shi, Y. Liang, Q. Lu and L. Ji, Selective aerobic oxidation of toluene to benzaldehyde catalyzed by covalently anchored *N*-hydroxyphthalimide and cobaltous ions, *Mol. Catal.*, 2021, **503**, 111440.
  - 26 M. Huda, K. Minamisawa, T. Tsukamoto, M. Tanabe and K. Yamamoto, Aerobic toluene oxidation catalyzed by subnano metal particles, *Angew. Chem.*, 2019, **131**(4), 1014–1018.
  - 27 G. Varga, Á. Kukovecz, Z. Kónya, P. Sipos and I. Pálkó, Green and selective toluene oxidation-Knoevenagel-condensation domino reaction over Ce-and Bi-based CeBi mixed oxide mixtures, *J. Catal.*, 2020, **381**, 308–315.
  - 28 G. Patel, A. R. Patel, T. L. Lambat, S. H. Mahmood and S. Banerjee, Rice husk derived nano-NiFe<sub>2</sub>O<sub>4</sub>@CAGC-catalyzed direct oxidation of toluene to benzyl benzoate under visible LED light, *FlatChem*, 2020, **21**, 100163.
  - 29 P. Paul, A. Ghosh, S. Chatterjee, A. Bera, S. M. Alam and S. M. Islam, Development of a polymer embedded reusable heterogeneous oxovanadium (IV) catalyst for selective oxidation of aromatic alkanes and alkenes using green oxidant, *Inorg. Chim. Acta*, 2019, **492**, 198–212.
  - 30 T. Karimpour, E. Safaei and B. Karimi, A supported manganese complex with amine-bis(phenol) ligand for catalytic benzylic C (sp<sup>3</sup>)-H bond oxidation, *RSC Adv.*, 2019, **9**(25), 14343–14351.
  - 31 P. Mohammadpour and E. Safaei, Catalytic C–H aerobic and oxidant-induced oxidation of alkylbenzenes (including toluene derivatives) over VO<sub>2</sub><sup>+</sup> immobilized on core-shell Fe<sub>3</sub>O<sub>4</sub>@SiO<sub>2</sub> at room temperature in water, *RSC Adv.*, 2020, **10**(40), 23543–23553.
  - 32 A. A. Ádám, S. Ziegenheim, Á. Papp, M. Szabados, Z. Kónya, Á. Kukovecz and G. Varga, Nickel Nanoparticles for Liquid Phase Toluene Oxidation–Phenomenon, Opportunities and Challenges, *ChemCatChem*, 2022, **14**(21), e202200700.
  - 33 S. Mehrabi-Kalajahi, A. O. Moghaddam, F. Hadavimoghaddam, M. A. Varfolomeev, A. L. Zinnatullin, I. Vakhitov, K. R. Minnebaev, D. A. Emelianov, D. Uchaev, A. Cabot and R. Il'dar, Entropy-stabilized metal oxide nanoparticles supported on reduced graphene oxide as a highly active heterogeneous catalyst for selective and solvent-free oxidation of toluene: a combined experimental and numerical investigation, *J. Mater. Chem. A*, 2022, **10**(27), 14488–14500.
  - 34 H. Wang, C. Cao, D. Li, Y. Ge, R. Chen, R. Song, W. Gao, X. Wang, X. Deng, H. Zhang and B. Ye, Achieving high selectivity in photocatalytic oxidation of toluene on amorphous BiOCl nanosheets coupled with TiO<sub>2</sub>, *J. Am. Chem. Soc.*, 2023, **145**(30), 16852–16861.
  - 35 H. Zhu, S. Ould-Chikh, H. Dong, I. Llorens, Y. Saih, D. H. Anjum, J. L. Hazemann and J. M. Basset, VO<sub>x</sub>/SiO<sub>2</sub> catalyst prepared by grafting VOCl<sub>3</sub> on silica for oxidative dehydrogenation of propane, *ChemCatChem*, 2015, **7**(20), 3332–3339.
  - 36 D. E. Keller, D. C. Koningsberger and B. M. Weckhuysen, Molecular structure of a supported VO<sub>4</sub> cluster and its

- interfacial geometry as a function of the SiO<sub>2</sub>, Nb<sub>2</sub>O<sub>5</sub>, and ZrO<sub>2</sub> support, *J. Phys. Chem. B*, 2006, **110**(29), 14313–14325.
- 37 A. M. Love, C. A. Carrero, A. Chiericato, J. T. Grant, S. Conrad, R. Verel and I. Hermans, Elucidation of anchoring and restructuring steps during synthesis of silica-supported vanadium oxide catalysts, *Chem. Mater.*, 2016, **28**(15), 5495–5504.
- 38 G. J. Colpas, B. J. Hamstra, J. W. Kampf and V. L. Pecoraro, Functional models for vanadium haloperoxidase: reactivity and mechanism of halide oxidation, *J. Am. Chem. Soc.*, 1996, **118**(14), 3469–3478.
- 39 G. Nallathambi, T. Ramachandran, V. Rajendran and R. Palanivelu, Effect of silica nanoparticles and BTCA on physical properties of cotton fabrics, *Mater. Res.*, 2011, **14**, 552–559.
- 40 M. C. Biesinger, B. P. Payne, A. P. Grosvenor, L. W. Lau, A. R. Gerson and R. S. Smart, Resolving surface chemical states in XPS analysis of first row transition metals, oxides and hydroxides: Cr, Mn, Fe, Co and Ni, *Appl. Surf. Sci.*, 2011, **257**(7), 2717–2730.
- 41 D. C. McKean, Individual CH bond strengths in simple organic compounds: effects of conformation and substitution, *Chem. Soc. Rev.*, 1978, **7**(3), 399–422.
- 42 D. Richard and N. M. Rendtorff, Kaolin group minerals under pressure: The study of their structural and electronic properties by DFT methods, *Appl. Clay Sci.*, 2022, **219**, 106444.
- 43 M. S. Prasad, K. J. Reid and H. H. Murray, Kaolin: processing, properties and applications, *Appl. Clay Sci.*, 1991, **6**(2), 87–119.
- 44 H. M. Davies and J. R. Manning, Catalytic C–H functionalization by metal carbenoid and nitrenoid insertion, *Nature*, 2008, **451**(7177), 417–424.
- 45 M. P. Doyle, R. Duffy, M. Ratnikov and L. Zhou, Catalytic carbene insertion into C–H bonds, *Chem. Rev.*, 2010, **110**(2), 704–724.
- 46 A. D. Becke, Density-functional thermochemistry. I. The effect of the exchange-only gradient correction. The, *J. Chem. Phys.*, 1992, **96**(3), 2155–2160.
- 47 C. Lee, W. Yang and R. G. Parr, Development of the Colle-Salvetti correlation-energy formula into a functional of the electron density, *Phys. Rev. B: Condens. Matter Mater. Phys.*, 1988, **37**(2), 785.
- 48 J. Cioslowski, A new population analysis based on atomic polar tensors, *J. Am. Chem. Soc.*, 1989, **111**(22), 8333–8336.
- 49 W. Stöber, A. Fink and E. Bohn, Controlled growth of monodisperse silica spheres in the micron size range, *J. Colloid Interface Sci.*, 1968, **26**(1), 62–69.
- 50 K. Chou and C. Chen, Preparation of monodispersed silica colloids using sol-gel method: COSOLVENT effect, *Ceram. Trans.*, 2005, **166**, 57.
- 51 H. D. Jang, Generation of silica nanoparticles from tetraethylorthosilicate (TEOS) vapor in a diffusion flame, *Aerosol Sci. Technol.*, 1999, **30**(5), 477–488.